Nanoscaled Microelectronics and Nanotechnology-Enabled Energy Systems For Aerospace and Robotic Applications

Sergey Edward Lyshevski*, Mamyrbek A. Beisenbi**,
Gulzhan Uskenbayeva**, Aliya Shukirova**, Janar Yermekbayeva** and Nurlan Mukataev**
*Department of Electrical and Microelectronic Engineering,Rochester Institute of Technology, Rochester,NY 14623 USA
E-mail: Sergey.Lyshevski@mail.rit.edu URL: http://people.rit.edu/seleee
**Department of System Analysis and Control, L. N. Gumilyov Eurasian National University,
Astana, Republic of Kazakhstan, aliya.shukirova@mail.ru

ABSTRACT

For autonomous and semi-autonomous micro air vehicles, minirobots, propulsion, remote sensing and other platforms, we study high-power and high-energy densities energy systems. These systems are designed using nanotechnology-enabled microelectronic, electronic, energy sources and energy storage components, devices and modules. Research and technology developments are performed for energy harvesting, management and storage. We apply and demonstrate key modules and components, such as: (1) Nanoscaled low-power microelectronics and sensors; (2) High-power-density semiconductor devices, circuit components and power electronics; (3) Nanotechnology-enabled solar cells; (4) Advanced energy storage devices; (5) Energy management system. The proposed solutions are substantiated by performing experimental studies. The compliance of the proposed technologies to radio-controlled mini air vehicles and robots is ensured. Proof-of-concept power systems are designed using specifications for *all-electric* autonomous aerospace, naval, robotic and security platforms.

Keywords: electronics, energy, nanotechnology

1. INTRODUCTION

Power adequacy, integrity and energy sustainability are essential to ensure functionality of propulsion, navigation, sensing, management and other systems in aerospace, land and underwater platforms. It is important to design, test and evaluate integrated self-sustained power systems for different platforms meeting application-specific requirements and specifications. Safety, affordability, energy density and other features can be ensured by using: (i) Nanotechnology-enabled components, devices and modules [1, 2]; (ii) Compliant *modular* organization; (iii) Advanced control schemes and management systems; (iv) Enabling energy harvesting and conversion solutions.

Advances in nanotechnology, microelectronics and micro-electromechanical systems (MEMS) [1, 2] result in commercialization and deployment of various minirobots, surface and air vehicles, etc. The energy module, which includes the energy source and other subsystems, is a key component. High-altitude, outer and deep space vehicles, robots as well as underwater platforms require specific modules and electronic devices which operate under extreme temperature, mechanical loads, interference and radiation. The controlled high-energy density power systems must be designed, tested and characterized.

We examine enabling inorganic and organic photovoltaic cells, nanotechnology-enabled electronic devices, front-end microelectronic components, efficient energy harvesting solutions, low-loss energy conversion and novel energy storage schemes. The controlled energy conversion, storage and distribution are accomplished by an energy management system. A coherent energy management implies consistent sensing, processing, optimization and control of energy conversion. Advanced sensing, data acquisition and processing are achieved by nanoscale electronics, optoelectronics and MEMS. The studied *modular* energy systems may operate in the range from milli-watts to hundreds of watts within continuous and pulse energy conversion and release capabilities. The proof-of-concept portable light-duty energy systems are tested and substantiated achieving a sufficient technology level.

2. SCALABLE AND *MODULAR* ENERGY SYSTEMS

With an overall objective to develop a scalable high-performance power system technology for high-energy density portable energy sources, the *modular* design is performed using nanoscale electronics and MEMS [1-4]. The power integrity, effective energy management and functionality must be guaranteed by matching compliant components and modules with the electric loads, energy harvesting and storage capabilities.

Figure 1 illustrates a *modular* power system which includes photovoltaic cells, power electronics (dc/dc converter, chargers, controllers, filters, sensors, etc.), MEMS, rechargeable battery and other modules.

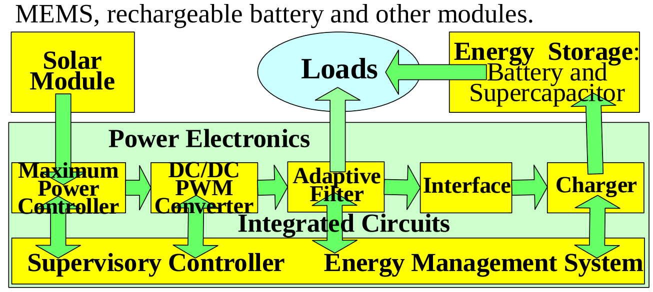

Figure 1: *Modular* self-sustained power system

One need to accommodate the application- and system-specific peak, continuous and pulse loading conditions, as well as time-varying *RLC* loads, such as electromechanical devices, antennas, communication components, electronics, etc. Therefore specific energy sources, converters and power electronic modules are used taking into account the rated and peak continuous and pulse loading conditions. Figure 2 documents the images of photovoltaic cells, super-capacitors, lithium-ion rechargeable battery, high-frequency high-efficiency dc/dc converters, etc. The varying *RLC* loads are the transmitters, receivers, permanent-magnet actuators and propulsion motors, servos, sensors and other devices [5-7].

Figure 2: Devices, components and modules of autonomous energy systems:
(a) Photovoltaic cells;
(b) Rechargeable supercapacitors and lithium ion battery;
(c) High-frequency *buck-boost* and *boost* converters;
(d) Loads: Electric motors, servos, transmitters and receivers.

3. Analysis and Control of Energy Systems

The nonlinear steady-state and dynamic analyses of energy systems component, such as photovoltaic cells and others, is reported in [3-5]. Depending on irradiation, incident angle, temperature and other factors, the output solar cell voltage $u_{\text{cell}}(t)$ varies. The output voltage, applied to the *i*th *RLC* load $u_{iRLC}(t)$, must be controlled and stabilized. The dc/dc *buck-boost* and *boost* converters are used [5,8]. The nanoscale electronics and nanotechnology-enabled components (MOSFETs, inductors and capacitors) are used. To stabilize the output voltage at the *RL* load, consider a one-quadrant *boost* converter with a filter. The converter schematics is shown in Figure 3 [5].

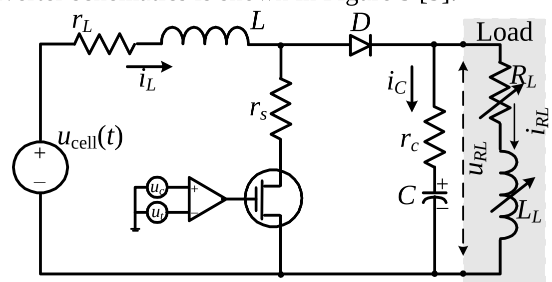

Figure 3: Controlled *boost* converter with the varying *RL* load

When the MOSFET is closed, using the currents and voltages as the state variables $\mathbf{x}=[u_C, i_L, i_{RL}]^T$, one has

$$\frac{du_C}{dt}=-\frac{1}{C}i_{RL},\quad \frac{di_L}{dt}=\frac{1}{L}\left[-(r_L+r_s)i_L+u_{cell}\right],$$
$$\frac{di_{RL}}{dt}=\frac{1}{L_L}\left[u_C-(R_L+r_c)i_{RL}\right].$$

When the MOSFET is open, the capacitor C is charged by the voltage source. The differential equations are

$$\frac{du_C}{dt}=\frac{1}{C}(i_L-i_{RL}),\quad \frac{di_L}{dt}=\frac{1}{L}\left[-u_C-(r_L+r_c)i_L+r_c i_{RL}+u_{cell}\right],$$
$$\frac{di_{RL}}{dt}=\frac{1}{L_L}\left[u_C+r_c i_L-(R_L+r_c)i_{RL}\right].$$

The comparator drives the MOSFET with the switching frequency f. Using the time when the MOSFET is *on* and *off*, one has $f=1/(t_{on}+t_{of})$. The voltage applied to the load u_{RL} is regulated by controlling the switching *on* and *off* durations t_{on} and t_{off}, respectively. The average voltage applied to the load depends on t_{on} and t_{off}. The duty cycle $d_D=\frac{t_{on}}{t_{on}+t_{off}}\in[0\ 1]$ varies between 0 and 1. Neglecting small resistances r_c and r_L, one obtains $\frac{u_{RL}}{V_d}=\frac{1}{1-d_D}$.

Using the *averaging* concept [5, 8], we have

$$\frac{du_C}{dt}=\frac{1}{C}(i_L-i_{RL}-i_L d_D),$$
$$\frac{di_L}{dt}=\frac{1}{L}\left[-u_C-(r_L+r_c)i_L+r_c i_{RL}+u_C d_D+(r_c-r_s)i_L d_D-r_c i_{RL} d_D+u_{cell}\right],$$
$$\frac{di_{RL}}{dt}=\frac{1}{L_L}\left[u_C+r_c i_L-(R_L+r_c)i_{RL}-r_c i_L d_D\right]. \tag{1}$$

TechConnect Briefs 2015, TechConnect.org, ISBN 978-1-4987-4728-8

The electronic components are fabricated using nanotechnologies. High-permeability and low eddy current losses ferrites are used in high-performance ferrite-core toroidal inductors. The soft, low coercivity and high-Q ferrites are the iron, zinc and manganese or nickel oxides. The high permeability soft ferrites $Mn_xZn_{(1-x)}Fe_2O_4$, high resistivity high-frequency $Ni_xZn_{(1-x)}Fe_2O_4$, and other ferrites are used. The structure and magnetic properties of $MnFe_2O_4$ ferrites depend on the preparation methods, such as the ceramic technique, combustion, co-precipitation, sol–gel and citrate. The citrate method gives the smallest lattice and ~15 nm particles, while the flash combustion results in ~40 nm. The ceramic technique results in the larger particle size, relative permeability ~2000, uniformity, etc.

In ferrite inductors, the relative permeability μ_r varies as a function of the load. For the toroidal inductors,

$$L = \mu \frac{N^2 h}{2\pi} \ln \frac{R_{\text{out}}}{R_{\text{in}}}, \tag{2}$$

where μ is the permeability, $\boldsymbol{\mu}=\mu_0\boldsymbol{\mu_r}=\mathbf{B}/\mathbf{H}$; μ_r is the relative permeability, $\mu_r=\mu_0^{-1}dB/dH$; B and H are the magnetic field density and intensity, $H=Ni/l$ [A/m]; l is the length; h is the thickness; R_{out} and R_{in} are the outer and inner radii.

The field intensity H and density B vary with current. The permeability μ also varies as a function of i. Using the nonlinear BH curve, one has $\mu_r(i, \frac{di}{dt}) = \mu_0^{-1}\frac{dB}{dH}$. Hence [9]

$$B(H, \tfrac{di}{dt}) = B_{\max}\tanh(aH - \operatorname{sgn}(\tfrac{di}{dt})bH_c),$$

$$L(i, \tfrac{di}{dt}) = B_{\max}c\left[1 - \tanh^2\left(ci - d\operatorname{sgn}(\tfrac{di}{dt})\right)\right], \tag{3}$$

where $B_{\max}$, a, b, c and d are the constants which depend on the BH curves of the nanostructured ferrites.

For a 2 mH ferrite toroidal inductor, N=60, $B_{\max}$=0.4 T, R_{out}=14 mm, R_{in}=7 mm, a=0.001, b=0.001, c=0.005 and d=0.05. The nonlinear magnetization curve and varying inductance $L(i)=f(i,di/dt)$ are reported in Figure 4. The nonlinear model (3) is used in design. The converter with the RL load is described by nonlinear differential equations

$$\frac{du_C}{dt} = \frac{1}{C}\left(i_L - i_{RL} - i_L d_D\right),$$

$$\frac{di_L}{dt} = \frac{1}{L(i_L)}\left[-u_C - (r_L + r_c)i_L + r_c i_{RL} + u_C d_D + (r_c - r_s)i_L d_D - r_c i_{RL} d_D + u_{cell}\right],$$

$$\frac{di_{RL}}{dt} = \frac{1}{L_L}\left[u_C + r_c i_L - (R_L + r_c)i_{RL} - r_c i_L d_D\right]. \tag{4}$$

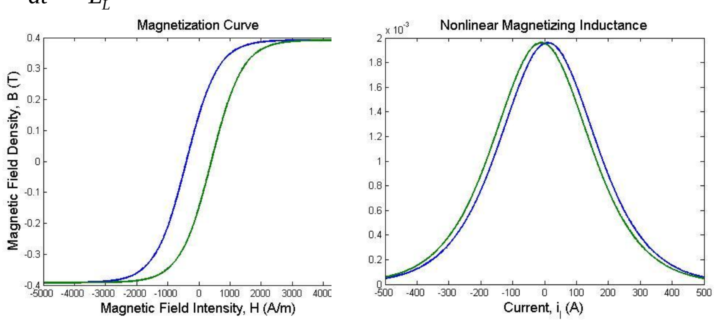

Figure 4: Inductor magnetization curve, and, nonlinear inductance $L(i, \frac{di}{dt}) = B_{\max}c\left[1 - \tanh^2\left(ci - d\operatorname{sgn}(\frac{di}{dt})\right)\right]$ as a function of current due to the varying permeability $\mu_r(i, \frac{di}{dt}) = \mu_0^{-1}\frac{dB}{dH}$.

4. EXPERIMENTAL RESULTS

We examine a high-energy density power system with high-efficiency solar cells and energy storage devices. The specific energy of super- and hybrid capacitors varies from ~1 to 30 W-h/kg, while for lithium-ion batteries, one may ensure ~200 W-h/kg. For different loads and loading conditions, depending on the spesified converter's output voltage $u_{\text{converter}}(t)$, we synthesize and verify nonlinear proportional-integral-derivative and sliding mode control laws [4, 10]. Using the tracking error

$e=u_{\text{reference}}(t) - u_{\text{converter}}(t)$,

we design and test the following control algorithms

$u(t)=k_pe + k_i\int edt + k_d de/dt$, $k_p>0$, $k_i>0$, $k_d=0$,

$u(t)=k_pe + k_{p1}e^{1/5} + k_i\int edt$, $k_p>0$, $k_{p1}>0$, $k_i>0$,

and $u=u_{\max}\tanh(k_pe + k_{p1}e^{1/5} + k_i\int edt)$, $k_p>0$, $k_{p1}>0$, $k_i>0$. (5)

Nonlinear control algorithms (5) are tested in the closed-loop energy systems with the RLC loads. The experimental results are documented in Figure 5 for the time-varying R and L. The evolution of $i_{RL}(t)$ and $u_{\text{converter}}(t)$ are given by the first and second oscilloscope's channels, respectively. The steady-state values and transient dynamics are reported for different reference voltages $u_{\text{reference}}(t)$ and time-varying loads. The tracking error $e(t)$ is less than 1% under the peak loads, and, the settling time is ~1 msec. At the rated load, the converter's efficiency is ~91%. The comparison of the experimental and analytic studies is summarized in Table 1.

Table 1. Comparison of Analytic and Experimental Steady-States

Assigned $u_{\text{reference}}$ which corresponds d_D	Analytic, modeling and simulation results $u_{\text{converter}}$ [V]	Experimental results (closed-loop system) $u_{\text{converter}}$ [V]
10.6	10.54	10.6
13.4	13.35	13.4
17.4	17.35	17.4
21	20.95	21

We depart from solutions reported in [11, 12]. A dynamic maximum power tracking algorithm and efficiency optimization scheme are implemented ensuring optimal energy conversion with minimal losses. The voltage stabilization, voltage tracking and high-efficiency energy management ensure optimal energy harvesting, conversion, distribution and storage. To achieve optimal performance, we minimize the performance functional J using the power losses $P_{j\text{Losses}}$, tracking error e_j, energy, energy transfer ΔE_j and other integrands for jth components and modules. In particular, using the weighting coefficients q_j, we have

$$J = \min_{P_{j\text{Losses}}, t, e_j} \max_{\eta} \int_{t_0}^{t_{\text{final}}} \left(\sum_j q_{P_j}\left|P_{j\text{ Losses}}\right| + \sum_j q_{e_j} t\left|e_j\right| + \sum_j q_{E_j}\left|\Delta E_j\right| \right) dt. \tag{6}$$

Using (6), performance and capabilities are measured by quantitative estimates, measures and metrics. Efficiency η, energy density, robustness, stability and other measures are examined in the full operating envelope. The consistent analytic measures and estimates are consistently used. Adequate cost, durability, integrity, modularity, storage capacity and other metrics are achieved.

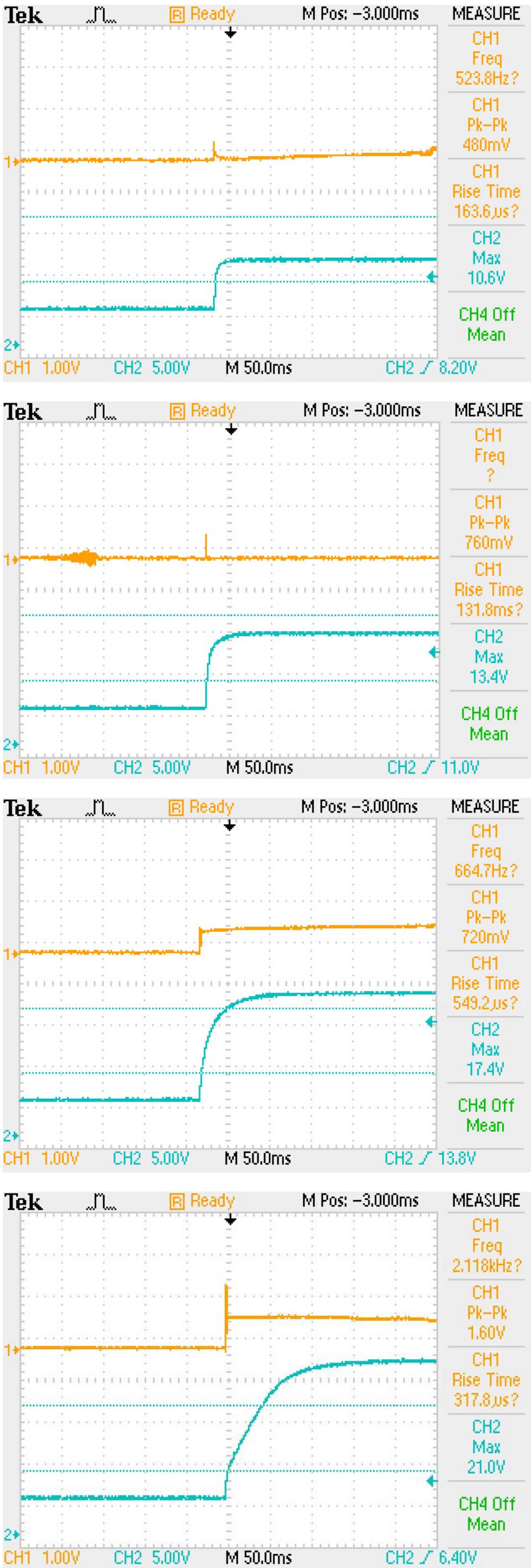

Figure 5. Dynamics of $i_{RL}(t)$ (top orange lines) and $u_{converter}(t)$ (bottom blue lines) for different reference voltages $u_{reference}(t)$ under varying *RL* loads: (a) $u_{reference}$=10.6 V; (b) $u_{reference}$=13.4 V; (c) $u_{reference}$=17.4 V; (d) $u_{reference}$=21 V.

5. CONCLUSIONS

For nanotechnology-enabled self-sustained power systems, we designed and substantiated a scalable *modular* technology. Advanced MEMS, electronic, photovoltaic and energy storage hardware solutions were used. Optimal energy conversion and management was ensured by designing practical *minimal-complexity* control laws. The proposed design ensures safety, affordability, accessibility, scalability, efficiency, effectiveness, simplicity, compliance, etc. The proposed concept meets specifications imposed in aerospace, automotive, biotechnology, consumer electronics, medical, naval, robotic, security and other applications. The effectiveness and applicability of *modular* portable energy systems were substantiated through experiments and technology transfer developments.

REFERENCES

[1] *International Technology Roadmap for Semiconductors*, 2005, 2007, 2009, 2011 and 2013 Editions, Semiconductor Industry Association, Austin, Texas, USA, 2015.

[2] *International Technology Roadmap for Semiconductors*, 2011 and 2013 Edition, *Micro-Electromechanical Systems* (*MEMS*), Semiconductor Industry Association, Austin, TX, USA, 2015.

[3] S. E. Lyshevski, "High-power density mini-scale power generation and energy harvesting systems," *Energy Conversion and Management*, vol. 52, pp. 46-52, 2011.

[4] T. C. Smith and S. E. Lyshevski, "*Clean* high-energy density renewable power generation systems with soft-switching sliding mode control laws," *Proc. IEEE Conf. Decision and Control*, Orlando, FL, pp. 836-841, 2011.

[5] S. E. Lyshevski, *Electromechanical Systems and Devices*, CRC Press, Boca Raton, FL, 2008.

[6] S. E. Lyshevski, "Motion control of electromechanical servo-devices with permanent-magnet stepper motors," *Mechatronics*, vol. 7, no. 6, pp. 521-536, 1997.

[7] S. E. Lyshevski, V. A. Skormin and R. D. Colgren, "High-torque density integrated electro-mechanical flight actuators," *IEEE Trans. Aerospace and Electronic Systems*, vol. 38, no. 1, pp. 174-182, 2002.

[8] S. E. Lyshevski, "Resonant converters: Nonlinear analysis and control," *IEEE Trans. Industrial Electronics*, vol. 47, no. 4, pp. 751-758, 2000.

[9] S. E. Lyshevski, "Precision control of mechatronic systems with electromagnetically-steered moving masses," *Int. Journal of Advanced Mechatronic Systems*, vol. 5, no. 5, pp. 306-316, 2013.

[10] S. E. Lyshevski, "Robust control of nonlinear continuous-time systems with parameter uncertainties and input bounds," *Int. Journal of Systems Science*, vol. 30, no. 3, pp. 247-259, 1999.

[11] J. Colomer, J. Brufau, P. Miribel, A. Saiz-Vela, M. Puig and J. Samitier, "Novel autonomous low power VLSI system powered by ambient mechanical vibrations and solar cells for portable applications in a 0.13µ technology," *Proc. Power Electronics Conf.*, pp. 2786-2791, 2007.

[12] G. Lijun, R. A. Dougal, S. Liu and A. Jotova, "Portable solar systems using a step-up power converter with a fast-speed MPPT and a parallel-configured solar panel to address rapidly changing illumination," *Proc. Applied Power Electronics Conf.*, pp. 520-523, 2007.